Available online at www.sciencedirect.com
SCIENCE DIRECT
Bioorganic & Medicinal Chemistry 14 (2006) 3553–3562
Bioorganic & Medicinal Chemistry

Structural and functional characterization of human microsomal prostaglandin E synthase-1 by computational modeling and site-directed mutagenesis

Xiaoqin Huang, Weili Yan, Daquan Gao, Min Tong, Hsin-Hsiung Tai* and Chang-Guo Zhan*

Department of Pharmaceutical Sciences, College of Pharmacy, University of Kentucky, 725 Rose Street, Lexington, KY 40536, USA

Received 15 December 2005; revised 6 January 2006; accepted 6 January 2006
Available online 24 January 2006

Abstract—Microsomal prostaglandin (PG) E synthase-1 (mPGES-1) has recently been recognized as a novel, promising drug target for inflammation-related diseases. Functional and pathological studies on this enzyme further stimulate to understand its structure and the structure–function relationships. Using an approach of the combined structure prediction, molecular docking, site-directed mutagenesis, and enzymatic activity assay, we have developed the first three-dimensional (3D) model of the substrate-binding domain (SBD) of mPGES-1 and its binding with substrates prostaglandin H2 (PGH2) and glutathione (GSH). In light of the 3D model, key amino acid residues have been identified for the substrate binding and the obtained experimental activity data have confirmed the computationally determined substrate–enzyme binding mode. Both the computational and experimental results show that Y130 plays a vital role in the binding with PGH2 and, probably, in the catalytic reaction process. R110 and T114 interact intensively with the carboxyl tail of PGH2, whereas Q36 and Q134 only enhance the PGH2-binding affinity. The modeled binding structure indicates that substrate PGH2 interacts with GSH through hydrogen binding between the peroxy group of PGH2 and the –SH group of GSH. The –SH group of GSH is expected to attack the peroxy group of PGH2, initializing the catalytic reaction transforming PGH2 to prostaglandin E2 (PGE2). The overall agreement between the calculated and experimental results demonstrates that the predicted 3D model could be valuable in future rational design of potent inhibitors of mPGES-1 as the next-generation inflammation-related therapeutic.

1. Introduction

Prostaglandin (PG) E2 is produced by a variety of cells and tissues, and exhibits potent diverse bioactivities.[1] Its production is mediated by three enzymatic reactions involving phospholipase A2 (PLA2), cyclooxygenase (COX), and PGE2 synthase (PGES). In this biosynthetic pathway, arachidonic acid (AA) releases from membrane phospholipids by cytosolic or secretory PLA2 and is converted to prostaglandin H2 (PGH2) by COXs. PGH2 is then isomerized to prostaglandin E2 (PGE2) by terminal PGES enzymes.[2] PGES enzymes, that lie downstream of COXs, occur in three forms in mammalian cells.[3–6] Among them, the microsomal and membrane-bound synthase (namely mPGES-1) has received much more attention and established as a novel drug target in the areas of inflammation, tumorigenesis, and bone disorders. Hence, mPGES-1 is involved in a number of diseases including arthritis, burn injury and pain diseases, atherosis, cancer, and even the exacerbation of Alzheimer's disease.[2,7–17] Recently reported studies have led to well characterization of its inducible distribution, expression, enzymatic kinetics, and biological and pathological functions.[18–28] The expression of mPGES-1 is up-regulated by proinflammatory stimuli and down-regulated by anti-inflammatory glucocorticoids, often in accordance with that of COX-2.[3,4,7,19,25,26] The protein mPGES-1 has been identified as the central switch during immune-induced pyresis,[20] and deletion of mPGES-1 would reduce inducible and basal PGE2 production and alter the gastric prostanoid profile.[24,26] Compared to its upstream enzymes, inhibition of mPGES-1 does not block normal functions of other PGs and, therefore, lacks the unexpected side effects produced by the inhibi-

Keywords: Prostaglandin; PGE2; mPGES-1; Protein structure; Molecular modeling; Mutagenesis; Binding affinity.
* Corresponding authors. Fax: +1 859 323 3575; e-mail: zhan@uky.edu

0968-0896/$ - see front matter © 2006 Elsevier Ltd. All rights reserved.
doi:10.1016/j.bmc.2006.01.010

tion of COXs, making it more attractive for the development of potential therapeutics, especially for the treatment of inflammation-related diseases.[3,29,30] However, no clinically useful inhibitor of mPGES-1 has been identified. So far, only two compounds, that is, the COX-2 inhibitor NS-398 (Chart 1) and 5-lipoxygenase-activating protein (FLAP) inhibitor MK-886 (Chart 1), have been found to be able to inhibit mPGES-1 with the IC_{50} values at micromole level.[2–4,29] It is highly desirable to develop more potent and selective inhibitors of mPGES-1 based on the structure and function of the enzyme for development of the next-generation therapeutics.

Initially, mPGES-1 was discovered as recombinant human microsomal glutathione-*S*-transferase (GST)-1-like 1 (MGST1-L1) and recognized as a member of membrane-associated proteins involved in eicosanoid and glutathione (GSH) metabolism (MAPEG) superfamily.[2,7,31,32] It shows significant homology with other MAPEG proteins, especially with the nearest subfamily member MGST1. Hydropathy analysis suggests that all the MAPEG proteins have similar three-dimensional (3D) and membrane-spanning topographic properties.[21,31–34] Site-directed mutagenesis revealed that R110 has an essential role in the catalytic function of mPGES-1, whereas the mutation on either R51 or R70 did not affect the activity.[2,3] Unfortunately, further structure–function investigation is restrained by the lack of the detailed 3D structure of this membrane-bound protein, which makes very difficult the structure-based design of drugs targeting mPGES-1. A two-dimensional (2D) electron projection map (with a resolution of 10 Å) of mPGES-1 revealed a trimer structure[21] which is very similar to that of MGST1, but the resolution of 10 Å is insufficient for the purpose of building a 3D model of mPGES-1. Nevertheless, the observed MGST1 trimer had a resolution of 3 Å for the 2D electron projection map and a resolution of 6 Å for the 3D map of MGST1 structure. The available structural information[35–39] has provided a stepping stone forward for building a 3D model of mPGES-1 structure with help from using modern molecular modeling techniques.

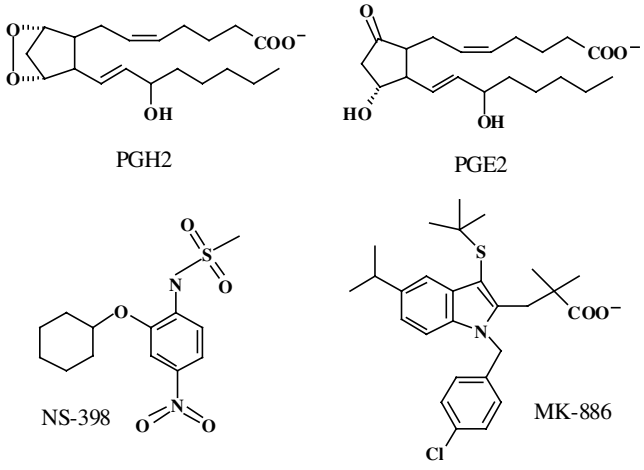

Chart 1. Molecular structures of PGH2, PGE2, NS-398, and MK-886.

In order to understand the molecular mechanism of the substrate binding, an 'ab initio' structure prediction approach has been developed in the present study to build a 3D model of the substrate-binding domain (SBD) of mPGES-1 by making use of the structural information available for both mPGES-1 and MGST1 of the MAPEG superfamily. Based on the 3D model of the SBD, key residues that are crucial for the substrate binding have been identified through further structural analysis and molecular docking. Site-directed mutagenesis and catalytic activity assay have been performed to validate the predicted 3D SBD model of the wild-type mPGES-1 and its mutants. The overall agreement between the computational and experimental results demonstrates some important structural features of the SBD of mPGES-1 and its binding with the substrates, providing a rational basis for future structure-based drug design.

2. Results

2.1. Structural models of the SBD of mPGES-1

The amino acid sequence alignment of mPGES-1 with MGST1 (Fig. 1) shows that four regions with high homology (>70%) can be assigned to four α-helices. These are α-helix A from sequence position #11 to #38, α-helix B from #78 to #93, α-helix C from #96 to #114, and α-helix D from #126 to #147. The longest loop between α-helix A and α-helix B contains typically conserved motifs. According to the geometric parameters used for the α-helices (Table 1), the explored 144,784 conformations derived from the initial topological model are screened down to 1934 candidate conformations. After the energy minimizations using the Sander module of Amber7.0 program, these 1934 candidates were clustered into four groups as shown in Figure 2. The 1232 candidates in the first group have positive energies, indicating that these 1232 candidate conforma-

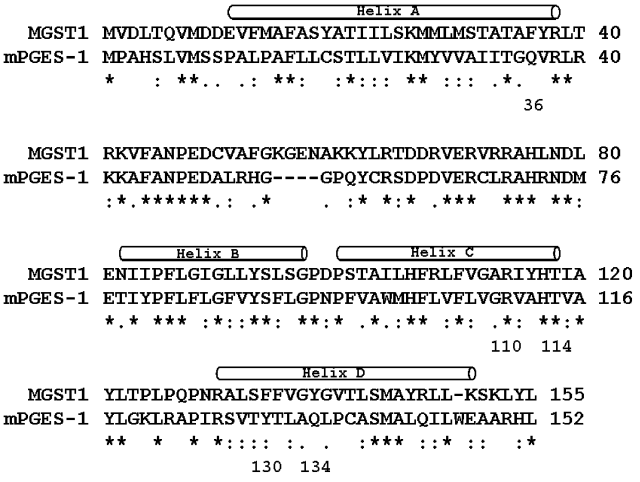

Figure 1. Sequence alignment of mPGES-1 with MGST1. Stars refer to identical residues, whereas filled period or double filled period refers to conservative substitutions. All these positions (with stars and filled periods) give the total homology of mPGES-1 with MGST1 as 73%. Helices of mPGES-1 are labeled. Mutated residues are numbered below the sequence.

Table 1. Geometric parameters used in generating topological model and applied as criteria in the conformational screening of the 144,784 initial candidates

Helix	A	B	C	D
Helix center (x,y plane)	11.0 Å, 16.0 Å	9.0 Å, 2.0 Å	0.0 Å, 0.0 Å	19.0 Å, 10.0 Å
Tilt angle (θ)	27.0°–37.0°	12.0°–20.0°	12.0°–22.0°	18.0°–18.0°
Helix-between distance	A–C: 19.4 Å	B–C: 9.2 Å		D–C: 21.5 Å
Helix arrangement	Anti-clockwise			
Membrane thickness	26.0 Å			
Kink of helix C toward helix A	3.0 Å			
Kink point to the C-terminal of helix C	11.0 Å			
Motion along the membrane normal (z axis)	±5.0 Å			
Relative rotation of each helix	±180.0°			
Self-rotation of each helix	±180.0°			
Orientation of hydrophobic residues	Toward membrane			

The screening led to 1934 candidates (the second set) for further consideration and then led to the finally selected 27 candidates (the final set of candidates).

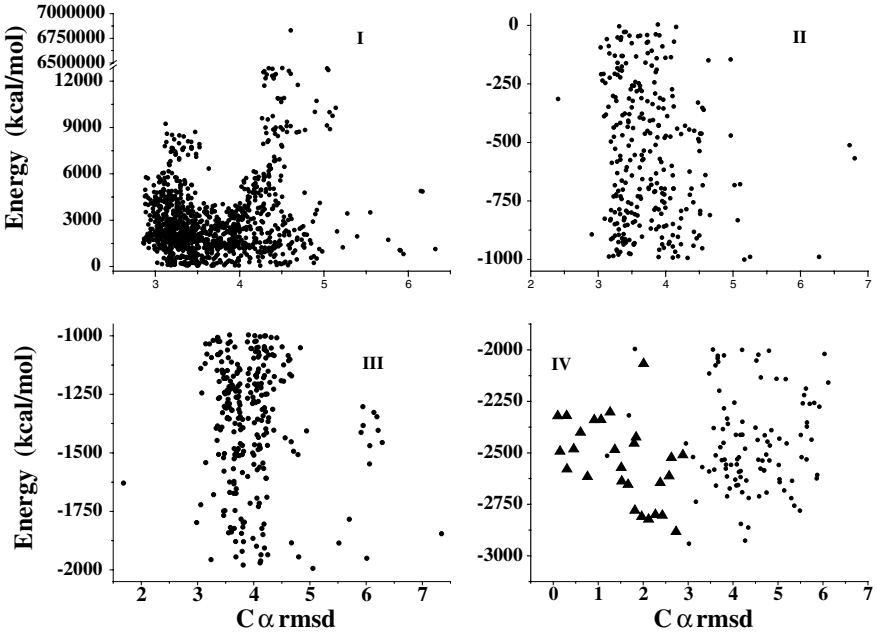

Figure 2. The second set of 1934 conformations clustered into four groups based on their energies and Cα rmsd values relative to the initial topological model. Group I (1232 candidates) was discarded due to their positive potential energies, whereas groups II (285 candidates), III (286 candidates), and IV (131 candidates) were used to derive the final set of 27 candidates. The selected 27 candidates are shown as triangles.

tions are energetically unfavorable and should be excluded. The energies calculated for the other groups of candidates are negative and become lower and lower from group II to group IV (see Fig. 2), showing the significant improvement of the positions of the side chains. This funnel-like adaptation of the four α-helix packing clearly shows both the energetic and geometric aspects dominating the formation of the final reasonable conformations of mPGES-1. Such folding-mimic process (Scheme 1) also helps to reduce the redundancy of the helix orientations. More strict geometric checking and evaluation of the root-mean-square deviation (rmsd) of the Cα positions from those in the initial topological model help us obtain eventual 27 best candidate conformations selected from group IV (Fig. 2). Although some of the other candidate structures also had small rmsd values and lower energies, those candidate structures were not selected because the helix packing was not as good as the selected 27 ones. Further, the helix packing was re-examined more strictly according to the geometric criteria (Table 1) and was finely tuned for the selected 27 candidates. Each of the finely tuned 27 candidate structures was energy-minimized again by using the Sander module of Amber7.0 program until the energy gradient criterion of 0.001 kcal/mol was achieved. The finally energy-minimized 27 candidate conformations with low energies and small rmsd values (Fig. 3) can be considered as the most possible conformations of the SBD of mPGES-1.

2.2. Complex model for mPGES-1 binding with PGH2 and GSH

The first test on the 27 structural models of the SBD of mPGES-1 was performed for their binding with substrates PGH2 and GSH, through molecular docking using both the binding site searching and interaction energy scoring. Each of the 27 structures was used to

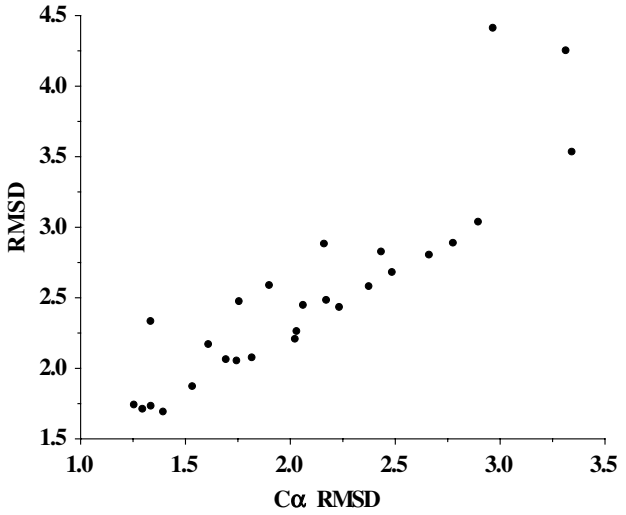

Figure 3. Conformational root-mean-square deviation (rmsd) from the initial topological model for the finally selected 27 candidates of the SBD model of mPGES-1.

perform molecular docking, with PGH2 and GSH separately. The calculated binding free energies of PGH2 with the SBD of mPGES-1 range from −4.1 to −8.3 kcal/mol. The corresponding values of the dissociation constant (K_d) fall between 995 and 0.768 μM (data not shown). The range of predicted K_d values covers the reported experimental values (~28, ~14, and ~160 μM) of the Michaelis–Menten constant (K_M).[5,18,21] We note that $K_d \neq K_M$ in theory. Nevertheless, $K_d \approx K_M$ under the widely used rapid-equilibration assumption[40–43] which assumes that the dissociation of the enzyme–substrate complex is much faster than the corresponding catalytic reaction. The catalytic reaction is characterized by the catalytic rate constant (k_{cat}). Based on the reported low k_{cat} values (1.8–50 S^{-1})[5,21] for mPGES-1, we consider $K_d \approx K_M$ in the discussion below. The finally selected complex model of mPGES-1 binding with both PGH2 and GSH substrates was the most satisfactory one with the best geometric matching (Fig. 4A) compared to the other complex candidates. The binding free energy (ΔG) calculated for the final complex model is −7.8 kcal/mol for PGH2 and −6.0 kcal/mol for GSH, respectively. Supposing $K_d \approx K_M$, the energetic results calculated for the final complex model predict a K_M value of 2.1 μM for PGH2 and a K_M value of 41.3 μM for GSH.

Based on the predicted complex model shown in Figure 4B, substrate PGH2 stays in a pocket formed by α-helices A, C, and D, with the two tails of PGH2 buried deeply. PGH2 has contacts with both hydrophilic and hydrophobic residues of mPGES-1. The most important interactions are around the carboxyl group on one tail of PGH2, which is surrounded by the polar side chain of Q36, positively charged side chain of R110, and side chain of T114 from α-helix C. The binding of these residues with PGH2 is associated with a network of electrostatic and hydrogen bonding interactions. Such an interacting mode is consistent with the reported experimental finding that R110S mutant of mPGES-1 completely lost the catalytic activity.[3] The hydroxyl group on the other tail of PGH2 interacts with side chain of Q134 through possible hydrogen bonding, and this hydrophobic tail is surrounded by side chains of V29, V30, I33, and V37, further strengthening the binding

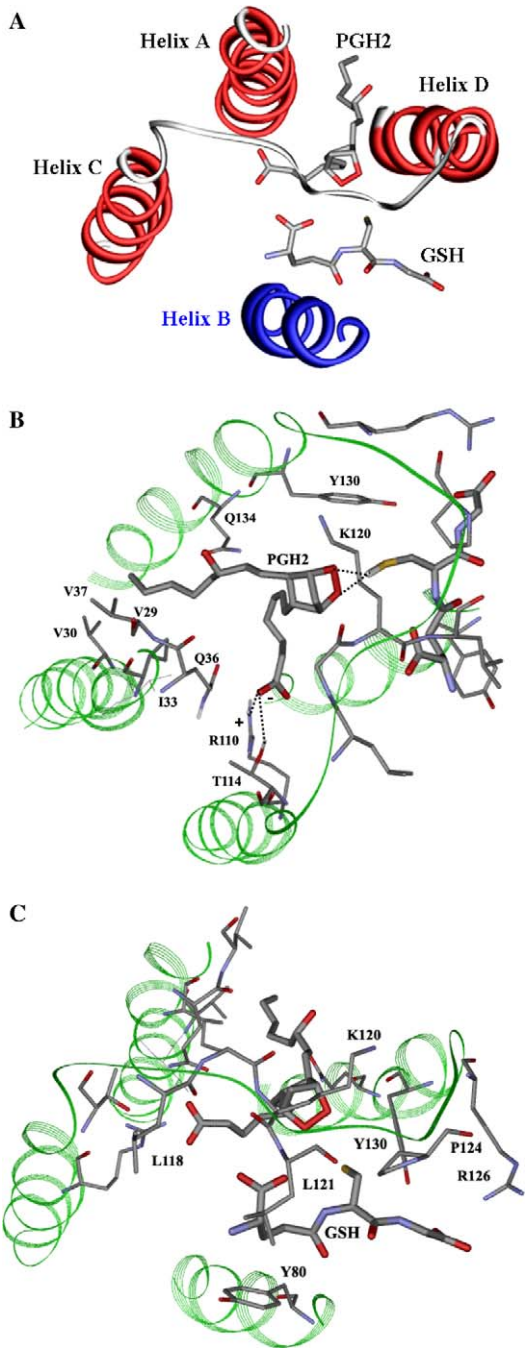

Figure 4. Finally optimized complex model of the SBD of mPGES-1 binding with substrates PGH2 and GSH. The SBD of mPGES-1 is represented as ribbon, and the two substrates are shown in stick. (A) Top view from outside of membrane. (B) PGH2 binding with the enzyme. Residues in the SBD of mPGES-1 within 5 Å around PGH2 are shown and labeled in stick, the electrostatic interaction is represented as the plus (+) and minus (−) signs, and the hydrogen bonding is indicated with dashed line. (C) GSH binding with the SBD of mPGES-1. Residues in the SBD of mPGES-1 within 5 Å around GSH are shown and labeled.

affinity of PGH2 with mPGES-1. As seen in the complex model, the two oxygen atoms forming the peroxy bridge of PGH2 also interact with the –SH group of GSH through hydrogen bonding. The head of the PGH2 molecule is close to the aromatic side chain of Y130 and is covered by hydrophobic part of the side chain of K120.

For the binding of GSH with the SBD of mPGES-1, as shown in Figure 4C, GSH is bound in a site nearby PGH2 under the loop between α-helices C and D. Compared to the location of PGH2, GSH is closer to surface of the protein. This site has not completely been modeled, as another α-helix C in a neighboring monomer could also be involved in the binding with GSH. The molecular docking with GSH was also guided by the insights obtained from the reported 2D and 3D electrodensity maps of mPGES-1 and MGST1.[21,35–39] Nevertheless, some useful features of the GSH binding still can be derived from the current model. As shown in Figure 4C, GSH is surrounded by Y80, L118, K120, L121, P124, R126, and Y130, and it is close to PGH2. Besides the thiol (–SH) group of GSH interacting with PGH2, the carboxyl group on the Gly-end of GSH interacts with a positively charged side chain of R126. Another carboxyl group on the γ-Glu-end of GSH points toward the backbone of K120 and L121. The packing of the –SH group of GSH and the head of PGH2 with the aromatic side chain of Y130 imply a possibly important role of Y130 in the catalytic function of mPGES-1.

2.3. PGH2 binding with mPGES-1 mutants

Based on the modeled SBD structure of mPGES-1 and the modeled binding structures with substrates, five key residues (i.e., Q36, R110, T114, Y130, and Q134) involved in the PGH2-binding site were selected for mutational studies in order to further test the predicted SBD model of mPGES-1. According to the 3D model of the substrate binding discussed above, the enzyme binding with substrate PGH2 should be weakened by such mutations as Q36E, R110T, T114V, Y130I, and Q134E. The binding affinities were estimated for the mutants of mPGES-1 by using the same method as used for the wild-type enzyme. The calculated results are summarized in Table 2 in comparison with available experimental data.

2.4. Membrane expression of mPGES-1 and its mutants

Based on the information of the structure prediction and modeling on substrate binding, five residues in the PGH2-binding site of mPGES-1 were selected for further site-directed mutagenesis studies. The substitutions for these five residues are Q36E, R110T, T114V, Y130I, and Q134E. The wild-type mPGES-1 was cloned from human placenta cDNA library by PCR techniques using specific sense and antisense primers of mPGES-1. The wild-type and the five mutants of mPGES-1 were expressed in M15 *Escherichia coli* cells. As the membrane proteins are very toxic to the host *E. coli*, a special strategy was used to produce sufficient amount of expression in order to favor the next activity assay. The best condition for expression was selected as 3 h at 37 °C. The membrane fractions were further analyzed by Western blotting using Ni-HRP as a detection system, which is more sensitive and accurate than the traditional analysis system of the primary and secondary antibodies. The results demonstrate that all the five mutants were expressed at a level comparable with that of the wild-type enzyme (Fig. 5).

Table 2. The calculated K_d values for PGH2 binding with the SBD of mPGES-1 in comparison with the experimentally derived kinetic data for wild-type mPGES-1 and the mutants

Enzyme	Calculated binding		Experimental K_M (μM)	
	ΔG (kcal/mol)	K_d (μM)	This work	Previously reported
Wild-type	−7.8	2.1[b]	130	14–160[a]
Q36E	−3.8	1600	∼1610	
Q134E	−4.7	359	∼734	

The experimental data were calculated by GraphPad Prism 4.01 program.

[a] The experimental K_M values reported previously by other groups are 28 μM (by Tanikawa et al.,[5]), 14 μM (by Ouellet et al.,[18]), and 160 μM (by Thoren et al.,[21]).

[b] The calculated k_d value is close to the range of the experimental K_M values (14–160 μM).

2.5. Enzymatic activity and kinetic data

The wild-type and the mutants of mPGES-1 were assayed for the enzymatic activity in the presence of PGH2 and GSH as substrates and the results are shown in Figure 6. The R110T mutation was designed to test mainly for its electrostatic and hydrogen bonding interactions with the carboxyl group of PGH2. This mutant retained only 17.8% catalytic activity of the wild-type, not totally abrogated as reported by Murakami et al.[3] The T114V mutant showed 21.3% activity of the wild-type mPGES-1, which is consistent with the computational prediction that the hydroxyl group of T114 side chain is involved in hydrogen bonding with PGH2. The Y130I mutant lost most of the enzymatic activity, indicating that this residue cannot tolerate any amino

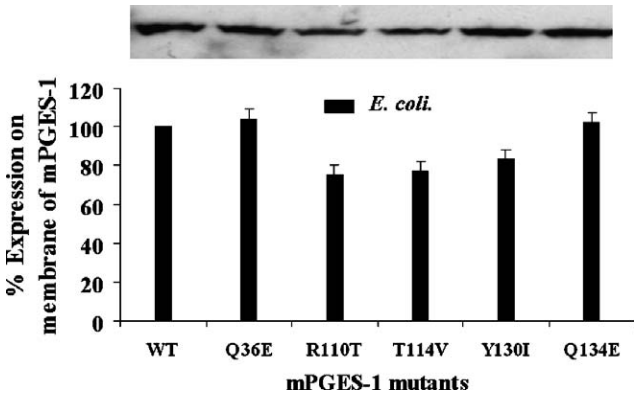

Figure 5. Cell membrane portion of mPGES-1 expression in *E. coli*. Bars represent the percentage of expression for the five mutants (Q36E, R110T, T114V, Y130I, and Q134E) relative to the wild-type (WT) of mPGES-1. These data are average results of three parallel repeats; only one set of Western blots is depicted in the figure.

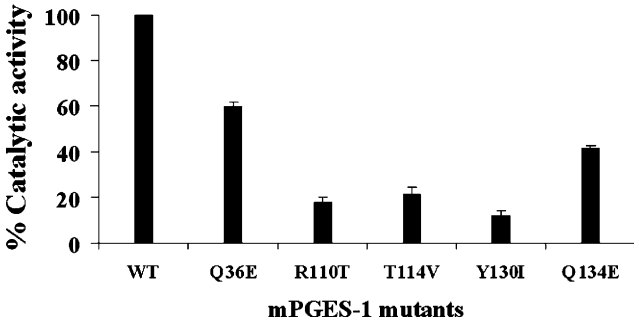

Figure 6. Relative enzymatic activity of mPGES-1 and its mutants. The relative activity is obtained by normalization from its expression level in Figure 5 and the wild-type served as a standard of 100 units. These experiments were repeated for three times.

acid change. This suggests that the role of Y130 in the reaction of PGH2 catalyzed by mPGES-1 is crucial. Q36E and Q134E mutants kept about 40–50% catalytic activity of the wild-type (Fig. 6), indicating that these two residues (Q36 and Q134) are not as important as the other three residues (R110, T114, and Y130) for the catalytic reaction.

The experimental results are listed in Table 2 and depicted in Figs. 6 and 7 for comparison with the computational predictions. As seen in Figure 6, each of the tested mPGES-1 mutants demonstrated a lower catalytic activity compared to the wild-type, which is qualitatively consistent with the predicted enzyme–substrate binding model. Quantitatively, the experimental kinetic constant K_M was determined only for the wild-type mPGES-1 and the Q36E and Q134E mutants, but the catalytic activity of the R110T, T114V, and Y130I mutants is too low for the measurement of kinetic constants. The correlation between the calculated K_d and the measured K_M for these two mutants is represented in Figure 8. For the wild-type mPGES-1, our experimental K_M value of 130 μM is comparable to the K_M values reported by Tanikawa et al. (28 μM),[5] Ouellet et al. (14 μM),[18] and Thoren et al. (160 μM).[21] The calculated K_M value of 2.1 μM is acceptable, although it is slightly smaller than the experimental range (14–160 μM). The binding constant (K_d) values predicted for the Q36E and Q134E mutants are in agreement with the experimental K_M values, although the errors of the experimental K_M values determined for these two mutants are expected to be very large because the used concentrations of PGH2 ($\leqslant$500 μM) are not sufficiently high due to the limitation of the solubility of PGH2. The overall qualitative agreement of the calculated results with the experimental data further supports our predicted 3D model of the substrate–enzyme binding.

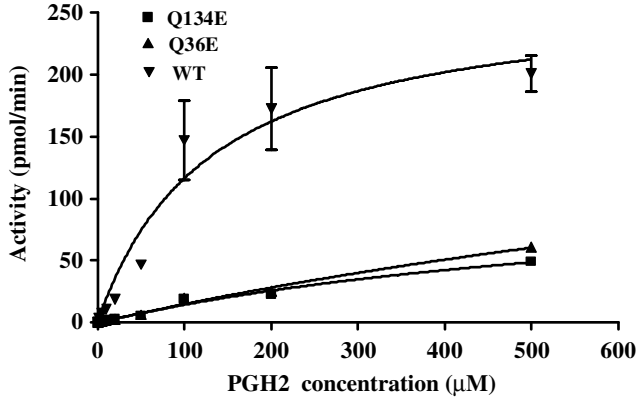

Figure 7. Experimentally measured K_M of mPGES-1 and its mutants. These data are the results of three repeats.

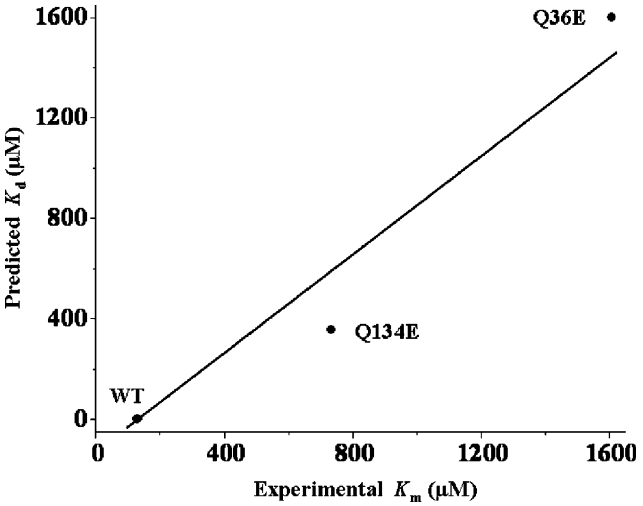

Figure 8. The calculated K_d values of PGH2 binding with wild-type mPGES-1 and its mutants in comparison with the experimentally derived K_M.

3. Discussion

Structural determination of membrane-spanning proteins is still exceedingly difficult by experimental methods such as X-ray diffraction and NMR. As a stimulating drug target, detailed information about the mPGES-1 structure and the relationship with its functions are sorely needed. In the present study, this need is partially satisfied by performing computational 3D structure predictions of the SBD of mPGES-1 and its binding with the substrates PGH2 and GSH, followed by wet experimental tests on the enzyme–substrate binding model predicted at atomic level. The 3D model reveals key amino acid residues, including Q36, R110, T114, Y130, and Q134, involved in the PGH2-binding site. Although the predicted 3D model is incomplete for the whole enzyme structure, for example, the exact packing of the α-helices and the long loop between α-helices A and B have not been modeled yet, the interrogation by wet experimental tests reveals that the predicted 3D model of the SBD binding with the substrates is reasonable. This first 3D model provides a good starting point for designing further structural and functional studies to shape more clearly the structural features of mPGES-1 as a drug target.

The current results (Figs. 6 and 7, and Table 2) obtained from the site-directed mutagenesis and enzymatic activity assay have confirmed two remarkable features of the predicted mPGES-1 binding with the substrates. One is

the relative position of the peroxy head of PGH2 to the –SH group of GSH in the binding site around residue Y130 of mPGES-1, reflecting the distinct role of Y130. Such a mode of the intermolecular interaction clearly explains why the catalytic function of mPGES-1 is GSH-dependent as observed in previous characterization studies on this enzyme.[5–7,18,21,28] The obtained binding mode also implies that the mPGES-1-catalyzed reaction of PGH2 could be initialized by the electrophilic attack of the –SH group of GSH at the peroxy oxygen of PGH2. Another feature is the contacts between the carboxyl tail of PGH2 and residues R110, T114, and Q36 of mPGES-1. Intermolecular interactions on this subsite reveal the role of residues R110, T114, and Q36 in the binding of mPGSE-1 with PGH2. R110 is conserved not only strictly for the MGST1 subfamily, but also for the whole superfamily of MAPEG,[31–33] suggesting a similar binding/catalytic role of this residue for all the members of this superfamily. The hydrogen bonding between the substrate and the subfamily-conserved residue T114 might imply a similar role of this residue for the members of MGST1 subfamily in the binding with the substrate. The indispensable role of the substitutable conserved Y130 demonstrates why mPGES-1 is specific for the reaction of PGH2. Amino acid residues #36 and #134 are not conserved even for the MGST1 subfamily, which is consistent with our observation that the catalytic activity of mPGES-1 did not dramatically decrease when these two residues were mutated.

In summary, the combined computational modeling and wet experimental tests have led to establishment of a reasonable three-dimensional (3D) model of the SBD of mPGES-1 and the understanding of mPGES-1 binding with the substrates. In the absence of an experimentally solved 3D structure, this first 3D model for mPGES-1 provides some detailed structural information concerning how this enzyme binds with the substrates at the atomic level. Based on the 3D model, further computational modeling and binding free energy calculations were performed to evaluate the substrate binding with Q36E, R110T, T114V, Y130I, and Q134E mutants of mPGES-1, followed by the site-directed mutagenesis and catalytic activity tests. The reasonable overall agreement between the calculated and experimental results demonstrates that the predicted 3D model could be valuable in future rational design of potent inhibitors of mPGES-1 for novel inflammation-related therapeutics.

4. Materials and methods

4.1. 'Ab initio' structure prediction

The sequence alignment was generated by using ClusterW with the Blosum scoring function.[44,45] The best alignment was selected according to not only the alignment score, but also the reciprocal position of the conserved residues. These included the conserved FANPED motif at positions #44 to #49, VERXXRAH motif from position #65 to #72, and R110. There was a gap of four residues from #55 to #58. The total homology is 73%, with the sequence identity of 38.8%. The membrane-spanning regions were defined based on the analysis of amino acid distribution and the homology with MGST1. The locations of substrates PGH2 and GSH in the SBD of mPGES-1 were thought to be similar to the corresponding locations of the substrates in the SBD of MGST1 revealed by the electron density map of MGST1.[38,39] Considering the low-resolution quaternary structure of mPGES-1, the 'ab initio' rationale (Scheme 1) began with the construction of topological model in which each helix was represented by Cα atoms, according to the structural parameters derived from the reported 2D and 3D electron projection maps of mPGES-1[21] and MGST1 (Table 1).[35–39] Here, the considered SBD is composed of α-helices A, C, and D from one monomer and α-helix B from another neighboring monomer. The present modeling study was focused only on the SBD, and the loop between α-helices A and B was not considered. The orientation of each α-helix was explored along three degrees of freedom, including the relative motion along the normal to the membrane, relative rotation among helices, and the helical self-rotation. A set of 144,784 candidate topological (Cα) structures were generated and, then, transformed into the corresponding residues of each helix. A set of criteria (Table 1) were used to screen the candidate structures and only 1934 candidate structures were kept for further consideration. The structures of these 1934 candidates were then fully optimized by performing the energy minimization using the Sander module of Amber7.0 program suite.[46] Initially, the loop between α-helices C and D was not considered. The energy minimization was carried out by using a non-bonded cutoff of 10 Å and conjugate gradient method, first with fixed backbone for 500 steps and then with constrained side chains for 300 steps. This was followed by energy minimization on the whole molecule for 1000 steps. Further energy minimization was performed after adding the loop between α-helices C and D. The energy minimization was continued until the root-mean-square deviation

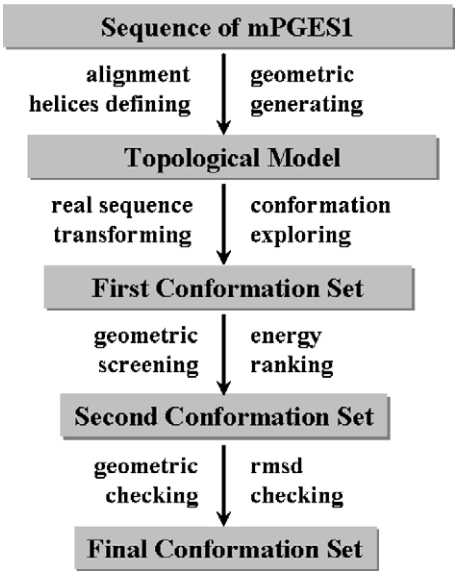

Scheme 1.

(rmsd) of the energy gradient was smaller than 0.001 kcal/mol/Å. Additional geometric screening was based on the structural compatibility among all the helices, as well as the overall deviation of the Cα atoms from the initial positions. This process eventually resulted in a set of 27 candidate structures (conformations) with a quite structural diversity and closely low energies. This set of molecular structures was viewed as the most possible conformations of the SBD of mPGES-1 and was used in further molecular docking tests.

4.2. Molecular docking and mutational calculation

The two native substrates PGH2 and GSH were treated as ligands and were separately docked into the aforementioned 27 candidate structures of the SBD of mPGES-1 by using the AutoDock 3.0.5 program.[47] The atomic charges used for these two ligands were the electrostatic potential (ESP)-fitted charges determined by performing first-principles electronic structure calculations using Gaussian03 program[48] at the HF/6-31G* level. The similar ESP-fitting calculations based on the first-principles electronic structure method were used in our previous computational studies of other protein–ligand systems and led to satisfactory binding structures.[49–53] The molecular docking was performed with a large population of randomly sampled ligand conformations and with random molecular translations using the Lamarkian genetic algorithm (LGA).[47] Through three types of operations in the LGA method, namely selection, mutation, and crossover, the substrate–enzyme matching quality was monitored and improved. On each docking site, the ligand conformation was searched by using the Solis and Wets local search method[54] in order to sample all the possible ligand conformations. Among a series of docking parameters, the size of the grid, in which both the enzyme and the ligand were embedded, was set to be 60 Å × 60 Å × 60 Å along the x, y, and z directions. This size of grid is large enough to cover all the protein atoms near the docking site and is also sufficient for calculating the long-range electrostatic interactions between the enzyme and ligand molecules. All the complex candidates were evaluated and ranked in terms of the binding free energies by using the standard energy score function implemented in the docking program and the geometric matching quality. The best complex candidate was selected from the docked structures according to the best geometric matching and the low binding free energy (high binding affinity). As the enzyme structure was kept rigid in the above docking process, the structure of this selected complex candidate was further refined through the energy minimization using the aforementioned Amber7.0 program, leading to the construction of the final complex structure.

Residue-based analysis was carried out for the obtained complex structure. Critical atomic contacts between the substrates and the enzyme were identified and the identified crucial residues binding with PGH2 include Q36, R110, T114, Y130, and Q134. In order to estimate individual contributions from these residues to the binding affinity with PGH2 and to know their possible role in the binding with the second substrate GSH, we further examined the substrate-bound SBD structures of five mPGES-1 mutants: Q36E, R110T, T114V, Y130I, and Q134E. The initial SBD structures of these mutants were generated based on the finally refined SBD structure of the wild-type by using the InsightII program (version 2002, Accelrys, San Diego, CA). The initial SBD structures of the substrate-bound mPGES-1 mutants were energy-minimized by using the same method as used for the substrate-bound wild-type mPGES-1. The substrate binding free energy (ΔG) with each mutant was calculated in the same way as we did for the binding with the wild-type enzyme.

All the computations were performed on a supercomputer (Superdome) at, University of Kentucky Center for Computational Sciences and on SGI Fuel workstations and a 34-processor IBM x335 Linux cluster in our own laboratory.

4.3. Vector, membrane, and cloning of mPGES-1

PQE40 expression vector, *E. coli* M15, and QIAprep Spin Plasmid miniprep Kit were from QIAgene. Restriction endonucleases were from New England BioLabs. The pfu polymerase was from Stratagene. Nickel-HRP was from Kirkegaard & Perry Laboratories (Gaithersburg, MA), polyvinylidene fluoride (PVDF) membrane was from Millipore Corp. ECL Western blotting detection system RPN 2132 was from Amersham Life Science. Oligonucleotide primers were synthesized by MWG Biotech. PGH2 and PGE2 were purchased from Cayman Chemicals. Other chemicals were from Sigma. The sequence of mPGES-1 was extracted from GenBank (Accession No. AF27740). The specific oligonucleotide primers to full length of mPGES-1 were synthesized to incorporate restriction sites (*Bam*HI and *Hin*dIII) into the 5′ and 3′ ends of the products. PCR was performed with 2 units Tag polymerase, 1 μl human placenta cDNA library as described previously.[55] The PCR product was subcloned into *E. coli* expression vector plasmid PQE40 at *Bam*HI and *Hin*dIII sites, which would express histidine X6-tagged mPGES-1. The ligated plasmids were transformed into XLI-Blue competent cells with the insertion confirmed by DNA sequencing.

4.4. Site-directed mutagenesis of mPGES-1

The internal primers were designed to contain sense and antisense mutagenic factors with mismatched codons in the wild-type sequence. All the mutations of mPGES-1 cDNA were performed by the quick change site-directed mutagenesis method.[56] The sequences of oligonucleotides used for mutagenesis were: Q36E: 5′-GTGG CCATCATCACGGGCGAAGTGAGGCTGCGGAA GAAG, 5′-CTTCTTCCGCAGCCTCACTTCGCCCG TGATGATGGCCAC; R110T: 5′-CTGGTCTTCCTC GTGGGCACTGTGGCACACACCGTGGCC and 5′-GGCCACGGTGTGTGCCACAGTGCCCACGA GGAAGACCAG; T114V: 5′-GTGGGCCGTGTGGC ACACGTCGTGGCCTACCTGGGGAAG and 5′-C TTCCCCAGGTAGGCCACGACGTGTGCCACAC GGCCCAC; Y130I: 5′-CCCATCCGCTCCGTGACC

ATCACCCTGGCCCAGCTCCCC and 5′-GGGGAG CTGGGCCAGGGTGATGGTCACGGAGCGGATG GG, Q134E: 5′-GTGACCTACACCCTGGCCGAGCT CCCCTGCGCCTCCATG and 5′-CATGGAGGCGC AGGGGAGCTCGGCCAGGGTGTAGGTCAC; where the underlines indicate the bases that were changed. Pfu DNA polymerase was used for PCR. The PCR products were treated with *Dpn*I endonuclease to digest the parental DNA template. All the mutant plasmids were transformed into XLI-Blue cells to amplify DNA. The DNA sequences of mutants were confirmed by sequencing.

4.5. Expression and preparation for the membrane fraction of mPGES-1 and its mutants in *E. coli*

The wild-type mPGES-1 and its mutant plasmids from XLI-Blue were transformed into M15 *E. coli* cells. Cells were grown in 500 ml TB media containing 100 μg/ml ampicillin and 25 μg/ml kanamycin at 37 °C with shaking at 270 rpm until OD reached 0.8. IPTG was added to a final concentration of 2 mM and cells were allowed to grow for additional 3 h at 37 °C. Cells were then harvested by centrifugation at 5000*g* for 15 min at 4 °C. The cell pellet was re-suspended in 15 mM Tris–HCl, pH 8.0, containing 0.25 M sucrose, 0.1 mM EDTA, and 1 mM reduced form glutathione. The cells were broken by sonication and then the cell lysate was cleared by centrifugation at 12,500*g* for 10 min. The supernatant then was centrifugated at 250,000*g* 4 °C for 1 h and the membrane pellet was re-suspended in PPGEG buffer (10 mM potassium phosphate, pH 7.0, 20% glycerol, 0.1 mM EDTA, and 1 mM reduced form glutathione). Total protein concentration of the membrane fraction was determined by Coomassie protein assay according to the manufacturer's instruction (Bio-Rad) with BSA as a standard.

4.6. SDS–PAGE and Western blotting

The *E. coli* membranes (50 μg) expressing the His-tagged wild-type and mutant mPGES-1 were subjected to SDS–PAGE on 15% polyacrylamide gel. The proteins were then electrophoretically transferred onto PVDF membranes. The membrane was blocked with 5% non-fat milk in TBS (30 mM Tris–HCl, pH 7.4, containing 120 mM NaCl) at room temperature for 1 h. After incubation for 2 h at room temperature with Nickel-HRP (1:500) in 5% non-fat milk in TBS, the membrane was washed three times with TBS containing 0.1% Tween 20. The immunoreactive bands were detected with ECL plus Western blotting detection system.

4.7. Activity assay for wild-type mPGES-1 and its mutants

Assays for mPGES-1 activity were performed on ice in 1.5 ml microfuge tubes using PGH2 as substrate. The reaction mixture (100 μl) contained: 100 mM sodium phosphate, pH 7.2, 2.5 mM GSH, and enzyme preparation. The reaction was initiated by the addition of 15 μM PGH2 from 20-fold concentrated stock solution in dry ethanol. After 8 min of incubation on ice, the reaction was quenched by the addition of 100 μl (2 mg/ml) $SnCl_2$ which rapidly reduced unreacted PGH2 to PGF2α. The non-enzymatic conversion of PGH2 to PGE2 was performed using PPGEG buffer devoid of enzyme. The reaction contents were 1:2500 diluted, from which 50 μl aliquot was used for quantification of PDE2 concentration by the EIA assay. The mPGES-1 activity was calculated using enzymatic conversion of PGH2 to PGE2 from total conversion subtracted by non-enzymatic conversion. When the saturation kinetics for PGH2 was determined, the activity was assayed with a fixed concentration of 2.5 mM GSH and 1–500 μM PGH2.

4.8. Calculation of kinetic data

The K_M values of wild-type mPGES-1 and its mutants were calculated by using the GraphPad Prism 4.01 program.

Acknowledgments

The research was supported in part by the Center for Computational Sciences (CCS) and the College of Pharmacy at University of Kentucky and by NIH Grant HL046.

References and notes

1. Serhan, C. N.; Levy, B. *Proc. Natl. Acad. Sci. U.S.A.* **2003**, *100*, 8609–8611.
2. Murakami, M.; Kudo, I. *Prog. Lipid Res.* **2004**, *43*, 3–35.
3. Murakami, M.; Naraba, H.; Tanioka, T.; Semmyo, N.; Nakatani, Y.; Kojima, Y.; Ikeda, T.; Fueki, M.; Ueno, A.; Oh-ishi, S.; Kudo, I. *J. Biol. Chem.* **2000**, *275*, 32783–32792.
4. Mancini, J. A.; Blood, K.; Guay, J.; Gordon, R.; Claveau, D.; Chan, C.-C.; Riendeau, D. *J. Biol. Chem.* **2001**, *276*, 4469–4475.
5. Tanikawa, N.; Ohmiya, Y.; Ohkubo, H.; Hashimoto, K.; Kangawa, K.; Kojima, M.; Ito, S.; Watanabe, K. *Biochem. Biophys. Res. Commun.* **2002**, *291*, 884–889.
6. Murakami, M.; Nakatani, Y.; Tanioka, T.; Kudo, I. *Prost. Lipid Med.* **2003**, *68/69*, 383–399.
7. Jakobsson, P.; Thoren, S.; Morgenstern, R.; Samuelsson, B. *Proc. Natl. Acad. Sci. U.S.A.* **1999**, *96*, 7220–7225.
8. Trebino, C. E.; Stock, J. L.; Gibbons, C. P.; Naiman, B. M.; Wachtmann, T. S.; Umland, J. P.; Pandher, K.; Lapointe, J. M.; Saha, S.; Roach, M. L.; Carter, D.; Thomas, N. A.; Durtschi, B. A.; McNeish, J. D.; Hambor, J. E.; Jakobsson, P. J.; Carty, T. J.; Perez, J. R.; Audoly, L. P. *Proc. Natl. Acad. Sci. U.S.A.* **2003**, *100*, 9044–9049.
9. Kojima, F.; Naraba, H.; Miyamoto, S.; Beppu, M.; Aoki, H.; Kawai, S. *Arthritis Res. Ther.* **2003**, *6*, R355–R365.
10. Kamei, D.; Murakami, M.; Nakatani, Y.; Ishikawa, Y.; Ishii, T.; Kudo, I. *J. Biol. Chem.* **2003**, *278*, 19396–19405.
11. Fahmi, H. *Curr. Opin. Rheumatol.* **2004**, *16*, 623–627.
12. Ozaki-Okayama, Y.; Matsumura, K.; Ibuki, T.; Ueda, M.; Yamazaki, Y.; Tanaka, Y.; Kobayashi, S. *Crit. Care Med.* **2004**, *32*, 795–800.
13. Kamei, D.; Yamakawa, K.; Takegoshi, Y.; Mikami-Nakanishi, M.; Nakatani, Y.; Oh-ishi, S.; Yasui, H.; Azuma, Y.; Hirasawa, N.; Ohuchi, K.; Kawaguchi, H.;

Ishikawa, Y.; Ishii, T.; Uematsu, S.; Akira, S.; Murakami, M.; Kudo, I. *J. Biol. Chem.* **2004**, *279*, 33684–33695.
14. Kojima, F.; Naraba, H.; Miyamoto, S.; Beppu, M.; Aoki, H.; Kawai, S. *Arthritis Res. Ther.* **2004**, *6*, R355–R365.
15. Cipollone, F.; Fazia, M.; Iezzi, A.; Ciabattoni, G.; Pini, P.; Cuccurullo, C.; Ucchino, S.; Spigonardo, F.; Luca, M.; Prontera, C.; Chiarelli, F.; Cuccurullo, F.; Mezzetti, A. *Arterioscler. Thromb. Vasc. Biol.* **2004**, 1259–1265.
16. Mabuchi, T.; Kojima, H.; Abe, T.; Takagi, K.; Sakurai, M.; Ohmiya, Y.; Uematsu, S.; Akira, S.; Watanabe, K.; Ito, S. *Neuroreport* **2004**, *15*, 1395–1398.
17. Subbaramaiah, K.; Yoshimatsu, K.; Scherl, E.; Das, K. M.; Glazier, K. D.; Golijanin, D.; Soslow, R. A.; Tanabe, T.; Naraba, H.; Dannenberg, A. J. *J. Biol. Chem.* **2004**, *279*, 12647–12658.
18. Ouellet, M.; Falgueyret, J. P.; Ear, P. H.; Pen, A.; Mancini, J. A.; Riendeau, D.; Percival, M. D. *Protein Expr. Purif.* **2002**, *26*, 489–495.
19. Catleya, M. C.; Chiversa, J. E.; Cambridgea, L. M.; Holdenb, N.; Slaterb, D. M.; Staplesa, K. J.; Bergmannc, M. W.; Loserd, P.; Barnesa, P. J.; Newton, R. *FEBS Lett.* **2003**, *547*, 75–79.
20. Engblom, D.; Saha, S.; Engstrom, L.; Westman, M.; Audoly, L. P.; Jakobsson, P. J.; Blomqvist, A. *Nat. Neurosci.* **2003**, *6*, 1137–1138.
21. Thoren, S.; Weinander, R.; Saha, S.; Jegerscho, J.; Pettersson, P. L.; Samuelsson, B.; Heber, H.; Hamberg, M.; Morgenstern, M.; Jakobsson, J. *J. Biol. Chem.* **2003**, *278*, 22199–22209.
22. Puxeddu, E.; Mitsutake, N.; Knauf, J. A.; Moretti, S.; Kim, H. W.; Seta, K. A.; Brockman, D.; Myatt, L.; Millhorn, D. E.; Fagin, J. A. *J. Biol. Chem.* **2003**, *278*, 52131–52138.
23. Wang, X.; Su, Y.; Deb, K.; Raposo, M.; Morrow, J. D.; Reese, J.; Paria, B. C. *J. Biol. Chem.* **2004**, *279*, 30579–30587.
24. Boulet, L.; Ouellet, M.; Bateman, K. P.; Ethier, D.; Percival, M. D.; Riendeau, D.; Mancini, J. A.; Methot, M. *J. Biol. Chem.* **2004**, *279*, 23229–23237.
25. Vazquez-Tello, A.; Fan, L.; Hou, X.; Joyal, J. S.; Mancini, J. A.; Quiniou, C.; Clyman, R. I.; Gobeil, F., Jr.; Varma, D. R.; Chemtob, S. *Am. J. Physiol. Regul. Integr. Comp. Physiol.* **2004**, *287*, R1155–R1163.
26. Shinji, Y.; Tsukui, T.; Tatsuguchi, A.; Shinoki, K.; Kusunoki, M.; Suzuki, K.; Hiratsuka, T.; Wada, K.; Futagami, T.; Miyake, K.; Gudis, K.; Sakamoto, C. *Am. J. Physiol. Gastrointest. Liver Physiol.* **2005**, *288*, G308–G315.
27. Gudis, K.; Tatsuguchi, T.; Wada, K.; Futagami, S.; Nagata, K.; Hiratsuka, T.; Shinji, Y.; Miyake, K.; Tsukui, T.; Fukuda, Y.; Sakamoto, C. *Lab. Invest.* **2005**, *85*, 225–236.
28. Parent, J.; Fortier, M. A. *Biol. Reprod.* **2005**, *73*, 36–44.
29. Thoren, S.; Jakobsson, P.-J. *Eur. J. Biochem.* **2000**, *267*, 6428–6434.
30. Flower, R. J. *Nat. Rev. Drug Dis.* **2003**, *2*, 179–191.
31. Jakobsson, P.-J.; Morgenstern, R.; Mancini, J.; Ford-hutchinson, A.; Persson, B. *Protein Sci.* **1999**, *8*, 689–692.
32. Jakobsson, P.-J.; Morgenstern, R.; Mancini, J.; Ford-hutchinson, A.; Persson, B. *Am. J. Respir. Crit. Care Med.* **2000**, *161*, S20–S24.
33. Ekstrom, L.; Lyrenas, L.; Jakobsson, P. J.; Morgenstern, R.; Kelner, M. J. *Biochem. Biophys. Acta* **2003**, *1627*, 79–84.
34. Hayes, J. D.; Flanagan, J. U.; Jowsey, I. R. *Annu. Rev. Pharmacol. Toxicol.* **2005**, *45*, 51–88.
35. Hebert, H.; Schmidt-Krey, I.; Morgenstern, F.; Murata, K.; Hirai, T.; Mitsuoka, K.; Fujiyoshi, Y. *J. Mol. Biol.* **1997**, *271*, 751–758.
36. Schmidt-Krey, I.; Lundqvist, G.; Morgenstern, R.; Hebert, H. *J. Struct. Biol.* **1998**, *123*, 87–96.
37. Schmidt-Krey, I.; Murata, K.; Hirai, T.; Mitsuoka, K.; Cheng, Y.; Morgenstern, R.; Fujiyoshi, Y.; Hebert, H. *J. Mol. Biol.* **1999**, *288*, 243–253.
38. Schmidt-Krey, I.; Mitsuoka, K.; Hirai, T.; Murata, K.; Cheng, Y.; Fujiyoshi, Y.; Morgenstern, R.; Hebert, H. *EMBO J.* **2000**, *19*, 6311–6316.
39. Holm, P. J.; Morgenstern, R.; Hebert, H. *Biochem. Biophys. Acta* **2002**, *1594*, 276–285.
40. Houston, J. B.; Galetin, A. *Arch. Biochem. Biophys.* **2005**, *433*, 351–360.
41. Ueda, S.; Oda, M.; Imamura, S.; Ohnishi, M. *Anal. Chem.* **2004**, *332*, 84–89.
42. Brown, A. E.; Grossman, S. H. *Arch. Biochem. Biophys.* **2004**, *57*, 166–177.
43. Anderson, W. B.; Board, P. G.; Anders, M. W. *Chem. Res. Toxicol.* **2004**, *17*, 650–662.
44. Thompson, J. D.; Higgins, D. G.; Gibson, T. J. *Nucleic Acids Res.* **1994**, *22*, 4673–4680.
45. Henikoff, S.; Henikoff, J. G. *Proc. Natl. Acad. Sci. U.S.A.* **1992**, *89*, 10915–10919.
46. Case, D. A.; Pearlman, D. A.; Caldwell, J. W.; Cheatham III, T. E.; Wang, J.; Ross, W. S.; Simmerling, C. L.; Darden, T.; Merz, K. M.; Stanton, R. V.; Cheng, A.; Vincent, J. J.; Crowley, M.; Tsui, V.; Gohlke, H.; Radmer, R.; Duan, Y.; Pitera, J.; Massova, I.; Seibel, G. L.; Singh, U. C.; Weiner, P.; Kollman, P. A. *AMBER 7.0*. University of California: San Francisco, CA, 2002.
47. Morris, G. M.; Goodsell, D. S.; Halliday, R. S.; Huey, R.; Hart, W. E.; Belew, R. K.; Olson, A. J. *J. Comput. Chem.* **1998**, *19*, 1639–1662.
48. Frisch, M. J.; Trucks, G. W.; Schlegel, H. B.; Scuseria, G. E.; Robb, M. A.; Cheeseman, J. R.; Montgomery, J. A., Jr.; Vreven, T.; Kudin, K. N.; Burant, J. C.; Millam, J. M.; Iyengar, S. S.; Tomasi, J.; Barone, V.; Mennucci, B.; Cossi, M.; Scalmani, G.; Rega, N.; Petersson, G. A.; Nakatsuji, H.; Hada, M.; Ehara, M.; Toyota, K.; Fukuda, R.; Hasegawa, J.; Ishida, M.; Nakajima, T.; Honda, Y.; Kitao, O.; Nakai, H.; Klene, M.; Li, X.; Knox, J. E.; Hratchian, H. P.; Cross, J. B.; Adamo, C.; Jaramillo, J.; Gomperts, R.; Stratmann, R. E.; Yazyev, O.; Austin, A. J.; Cammi, R.; Pomelli, C.; Ochterski, J. W.; Ayala, P. Y.; Morokuma, K.; Voth, G. A.; Salvador, P.; Dannenberg, J. J.; Zakrzewski, V. G.; Dapprich, S.; Daniels, A. D.; Strain, M. C.; Farkas, O.; Malick, D. K.; Rabuck, A. D.; Raghavachari, K.; Foresman, J. B.; Ortiz, J. V.; Cui, Q.; Baboul, A. G.; Clifford, S.; Cioslowski, J.; Stefanov, B. B.; Liu, G.; Liashenko, A.; Piskorz, P.; Komaromi, I.; Martin, R. L.; Fox, D. J.; Keith, T.; Al-Laham, M. A.; Peng, C. Y.; Nanayakkara, A.; Challacombe, M.; Gill, P. M. W.; Johnson, B.; Chen, W.; Wong, M. W.; Gonzalez, C.; Pople, J. A. *Gaussian 03*, Revision A.1, Gaussian, Inc., Pittsburgh, PA, 2003.
49. Zhan, C.-G.; Norberto de Souza, O.; Rittenhouse, R.; Ornstein, R. L. *J. Am. Chem. Soc.* **1999**, *121*, 7279–7282.
50. Koca, J.; Zhan, C.-G.; Rittenhouse, R.; Ornstein, R. L. *J. Am. Chem. Soc.* **2001**, *123*, 817–826.
51. Zhan, C.-G.; Zheng, F.; Landry, D. W. *J. Am. Chem. Soc.* **2003**, *125*, 2462–2474.
52. Hamza, A.; Cho, H.; Tai, H.-H.; Zhan, C.-G. *J. Phys. Chem. B* **2005**, *109*, 4776–4782.
53. Hamza, A.; Cho, H.; Tai, H.-H.; Zhan, C.-G. *Bioorg. Med. Chem.* **2005**, *13*, 4544–4551.
54. Solis, F. J.; Wets, R. J. B. *Math. Oper. Res.* **1981**, *6*, 19–30.
55. Ensor, C. M.; Zhang, H.; Tai, H.-H. *Biochem. J.* **1998**, *330*, 103–108.
56. Braman, J.; Papworth, C.; Greener, A. *Methods Mol. Biol.* **1996**, *57*, 31–44.